ACS central science

Research Article

Cite This: ACS Cent. Sci. 2018, 4, 397−404

Pendant Hydrogen-Bond Donors in Cobalt Catalysts Independently Enhance CO_2 Reduction

Alon Chapovetsky,[†,‡] Matthew Welborn,[‡,§] John M. Luna,[†] Ralf Haiges,[†] Thomas F. Miller III,[*,§] and Smaranda C. Marinescu[*,†]

[†]Department of Chemistry, University of Southern California, Los Angeles, California 90089, United States

[§]Division of Chemistry and Chemical Engineering, California Institute of Technology, Pasadena, California 91125, United States

Supporting Information

ABSTRACT: The bioinspired incorporation of pendant proton donors into transition metal catalysts is a promising strategy for converting environmentally deleterious CO_2 to higher energy products. However, the mechanism of proton transfer in these systems is poorly understood. Herein, we present a series of cobalt complexes with varying pendant secondary and tertiary amines in the ligand framework with the aim of disentangling the roles of the first and second coordination spheres in CO_2 reduction catalysis. Electrochemical and kinetic studies indicate that the rate of catalysis shows a first-order dependence on acid, CO_2, and the number of pendant secondary amines, respectively. Density functional theory studies explain the experimentally observed trends and indicate that pendant secondary amines do not directly transfer protons to CO_2, but instead bind acid molecules from solution. Taken together, these results suggest a mechanism in which noncooperative pendant amines facilitate a hydrogen-bonding network that enables direct proton transfer from acid to the activated CO_2 substrate.

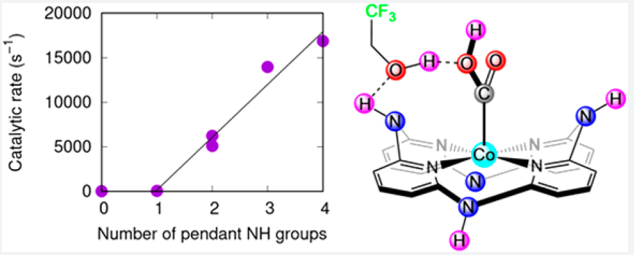

INTRODUCTION

The catalytic conversion of carbon dioxide (CO_2) into chemical fuels holds promise for mitigating the adverse effects of fossil fuels on the environment.[1−9] In nature, the selective and reversible conversion of CO_2 to carbon monoxide (CO) is catalyzed by the enzyme CO-dehydrogenase (CODH) through the transfer of two electrons and two protons.[2,10] Binding and reduction of CO_2 occur through bifunctional activation by the two metal centers in the NiFe cluster and additional stabilization through hydrogen bonding from appropriately positioned residues, as revealed by structural studies of the active site.[11] These studies suggest that a transition-metal center surrounded by ligands with pendant proton donors is an effective design motif for artificial CO_2 reduction catalysts.

Pendant proton donors also facilitate catalysis of the hydrogen evolution reaction (HER). In nature, HER occurs at the FeFe-hydrogenase (FFH) active site, which—like CODH—exhibits two metal centers surrounded by pendant proton donors.[2,12] In FFH, protons are shuttled to and from the active metal center by the secondary amine of an azadithiolene moiety.[13] The structure of this active site has inspired the development of nickel phosphine complexes bearing pendant tertiary amines; these complexes have proven to be extremely active HER electrocatalysts, with a mechanism that involves the cooperative interaction of H_2 with both the metal center and the pendant amines.[4,14,15]

Incorporation of pendant proton donors into molecular catalysts has only recently been explored in the context of CO_2 reduction. The electrochemical CO_2-to-CO activity of iron porphyrin and metal bipyridine complexes was shown to increase with the incorporation of pendant phenol or trimethylanilinium moieties into the ligand scaffold.[6,16−24] The prepositioned phenol groups were proposed to stabilize the initial $Fe^{(0)}$−CO_2 adduct through H-bonding, as confirmed by density functional theory (DFT) studies, and to facilitate the intramolecular protonation.[17,18] Nickel and cobalt phosphine complexes bearing pendant tertiary amines have been recently shown to catalyze the electrochemical conversion of CO_2 to formic acid, as well as the reverse reaction.[25−27] Additionally, nickel and cobalt cyclam systems bearing four secondary amines were shown to electrochemically convert CO_2 into CO.[1,3,5,9,28−33] DFT studies proposed that CO_2 is activated through cooperative hydrogen-bonding interactions between the Ni-bound substrate and the secondary amines in the ligand framework.[9,30,34,35] Electrochemical studies of nickel complexes supported by mono-, di-, tri-, and tetramethylated cyclam ligands revealed that both the catalytic activity and faradaic efficiency for CO_2-to-CO conversion decrease upon methylation of the ligand framework.[30,35] Methylation of the cyclam ligands impacts both the first and second coordination spheres of the nickel complexes. Hence, the effects of the two cannot be decoupled and a direct correlation between the number of pendant proton donors and the activity of the catalyst could not be established.

Received: December 19, 2017
Published: February 23, 2018

DOI: 10.1021/acscentsci.7b00607
ACS Cent. Sci. 2018, 4, 397−404

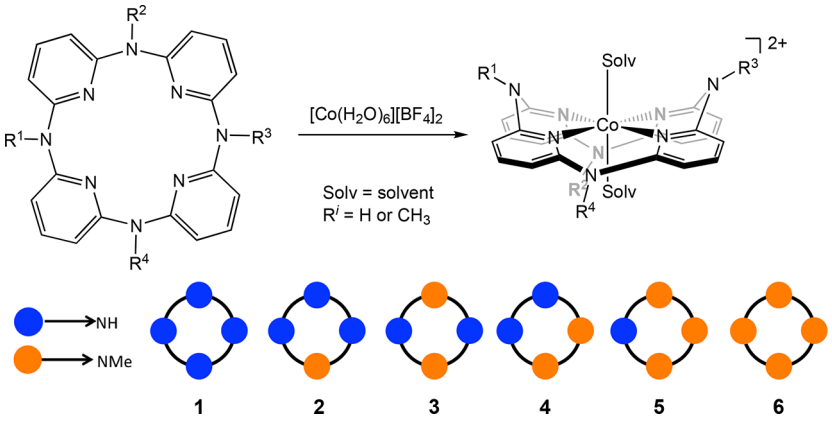

Figure 1. Syntheses of complexes $\mathbf{1}^{(II)}$–$\mathbf{6}^{(II)}$. The oxidation state of the cobalt center in each complex is indicated by the superscript.

We previously reported a cobalt complex bearing four pendant secondary amine (NH) groups incorporated in the ligand scaffold that is an efficient electrocatalyst for the selective reduction of CO_2 to CO.[36] Methylation of all four secondary amines produces a 300-fold reduction in activity, indicating that the pendant amines are important for catalysis.[36] Unlike the metal cyclam series, the pendant amines lie completely outside of the primary coordination sphere of the metal center, allowing for isolation of the role of pendant protons. In addition, our ligand framework allows for discrete control over the number and configuration of the proton donors present in the outer sphere of the metal center without impacting its primary coordination environment.[37] These structural features enable us to decouple the roles of the first and second coordination spheres in a systematic and well-controlled manner. In the current work, we investigate an expanded series of cobalt aminopyridine compounds through the synthesis of mono-, 1,2-di-, 1,3-di-, and trimethylated ligand scaffolds (Figure 1). We combine experimental and theoretical approaches to elucidate the mechanism by which these catalysts bind and reduce CO_2 in an effort to isolate and quantify the effect of pendant amine protons on catalysis. This work provides new design principles for tuning the effect of the second coordination sphere on CO_2 reduction.

RESULTS

Syntheses and Physical/Electrochemical Characterization. Complexes $\mathbf{2}^{(II)}$ through $\mathbf{5}^{(II)}$ are synthesized using procedures similar to those reported for complexes $\mathbf{1}^{(II)}$ and $\mathbf{6}^{(II)}$ (Figure 1).[36] Single crystal X-ray diffraction studies reveal a consistent motif for all six complexes, with a cobalt metal center coordinated by four pyridines in a square planar fashion (Figures S1–S4, Tables S1–S4). Complexes $\mathbf{1}^{(II)}$–$\mathbf{6}^{(II)}$ adopt a saddle conformation in which each set of opposing amines points outward from the face of the complex. There is little variance in the $Co-N_{Pyridine}$ and $Co-N_{PendantAmine}$ bond lengths (1.95(2) Å and 3.06(4) Å on average, respectively) among the complexes. The measured pK_a values of complexes $\mathbf{1}^{(II)}$–$\mathbf{5}^{(II)}$ range between 2.48 and 3.10 (Table 1). Given their acidity, complexes $\mathbf{1}^{(II)}$–$\mathbf{5}^{(II)}$ are expected to be singly deprotonated in solution.[38] Attempts to further titrate samples $\mathbf{1}^{(II)}$–$\mathbf{5}^{(II)}$ in order to obtain additional pK_a values have been unsuccessful and resulted in decomposition. Electrochemical characterization of complexes **1**–**6** under N_2 reveals a reversible one-electron reduction with $E_{1/2}$ between −1.41 and −1.65 V vs $Fc^{+/0}$, attributed to the $Co^{(II)}/Co^{(I)}$ couple (Table 1, Figures S5–S14). An irreversible reduction feature is observed between −2.46 and −2.87 V vs $Fc^{+/0}$ and is attributed to the reduction of $Co^{(I)}$ to $Co^{(0)}$ (Figures S15–S19). At fast scan rates, complexes **1** and **2** show a positively shifted return oxidation, indicating that the couple is slow or involves a chemical rearrangement.

Table 1. Parameters for Complexes 1–6[a]

complex	$E_{1/2}(CoL^{2+/+})$ vs $Fc^{+/0}$	$E(CoL^{+/0})$ vs $Fc^{+/0}$	i_{cat}/i_p	k_{obs} (s^{-1})	FE (%)	pK_a
1	−1.65	−2.46	208.8	16,900	98	2.74
2	−1.66	−2.73	189.9	14,000	98	2.66
3	−1.53	−2.41	130.0	6,200	98	2.53
4	−1.52	−2.41	113.7	5,200	98	3.10
5	−1.44	−2.87	11.4	50	90	2.48
6	−1.41	−2.58	7.7	20	36	na

[a]Reduction potentials (E), normalized current densities (i_{cat}/i_p), catalytic rate constants (k_{obs}), Faradaic efficiencies (FE), and pK_a values for complexes **1**–**6**.

Mechanistic Studies of CO_2 Reduction Catalysis. To explain the 300-fold decrease in activity between complexes **1** and **6**, we previously proposed that CO_2 binding and catalysis in complex **1** occurs through the formation of a $Co^{(0)}$–CO_2 adduct, which is stabilized through two intramolecular H-bonding interactions from the pendant secondary amines.[36] This stabilization cannot occur for **6**, which lacks pendant secondary amines. The current study provides additional kinetic analysis of complexes **1** and **6**, as well as the additional context of complexes **2**–**5**, to elucidate the mechanism by which these catalysts bind and reduce CO_2.

Electrochemical reduction of **1** under varying concentrations of CO_2 (0 to 0.2 M) gives rise to current increases at potentials near that of $Co^{(I)}/Co^{(0)}$ reduction (Figure S20). The potential corresponding to the maximum current displays a positive shift with increased [CO_2]. This behavior is Nernstian and suggests a thermodynamically favorable interaction between $\mathbf{1}^{(0)}$ and CO_2, consistent with the formation of a CO_2-bound preassociation complex.[36] Controlled potential electrolysis (CPE) studies of **1** under CO_2 saturation generate trace amounts of CO, suggesting that even in the absence of any added proton donors the CO_2-to-CO conversion occurs. This result is in agreement with the pK_a measurements, which indicate that the NH moieties are acidic. Hence, useful quantitative CO_2 binding constants cannot be extracted from the positive shifts observed in the titration of complexes **1**–**5** with CO_2.[32,39]

DOI: 10.1021/acscentsci.7b00607
ACS Cent. Sci. 2018, 4, 397–404

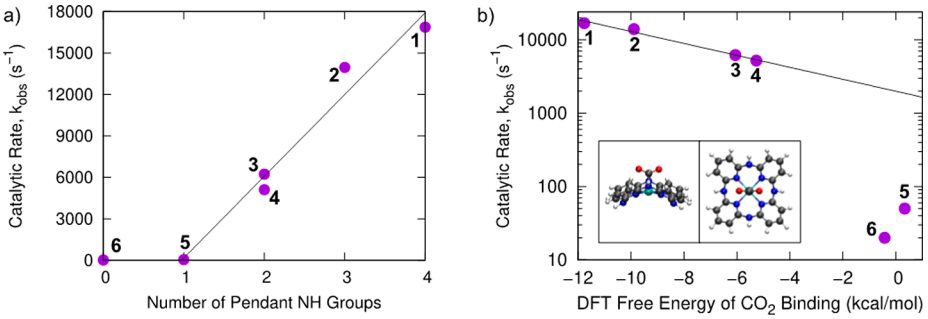

Figure 2. (a) Experimental catalytic rate constants, k_{obs} (s^{-1}), as a function of the number of pendant secondary amines for complexes **1**−**6** measured in the presence of 1.5 M TFE and under CO_2 saturation at a scan rate of 100 mV/s. Rates are obtained from the plateau current. A linear fit (R^2 = 0.97) is shown in gray for complexes **1**−**5**. (b) Experimental catalytic rate constants (log scale) versus computed CO_2 binding energy for complexes $\mathbf{1}^{(I)}$−CO_2 through $\mathbf{6}^{(I)}$−CO_2. The best-fit line (R^2 = 0.97) for complexes $\mathbf{1}^{(I)}$−CO_2 through $\mathbf{4}^{(I)}$−CO_2 is shown in gray. Inset: side and top views of the geometry of complex $\mathbf{1}^{(I)}$−CO_2. Atom colors: H = white, C = gray, N = blue, O = red, and Co = cyan.

Titration of **1** with acid (2,2,2-trifluoroethanol, TFE) under CO_2 saturation gives rise to a series of plateaus with a maximum at −2.7 V vs $Fc^{+/0}$ (Figure S24, Table S6). The normalized peak catalytic current (i_{cat}/i_p) is related to the rate of the catalytic reaction, as described in more detail in Supporting Information eqs 1−5. The i_p values used correspond to the peak current obtained from either the irreversible $Co^{I/0}$ reduction or the reversible $Co^{II/I}$ couple. A plot of the catalytic rate constant, k_{obs}, vs [TFE] shows a linear correlation, indicating a reaction that is first order in acid (Figure S25). A titration with CO_2 at 1.2 M TFE followed by an analogous analysis produces a linear correlation between the catalytic rate constant and [CO_2], consistent with a reaction that is first order in CO_2 (Figures S22 and S23, Table S5). Titrations with TFE-d_3 are performed under CO_2 saturation (Figures S27−S29, Table S7), giving rise to a H/D kinetic isotope effect (KIE) of 1.4(2). This result suggests that protons are involved in the rate-limiting step (RLS).

Complexes **2**−**6** are studied in a similar manner (Table 1, Figures S30−S41). All complexes exhibit a scan-rate independent, linear relationship between the rate and [TFE], indicative of a reaction that is first order in [TFE]. Controlled potential electrolysis (CPE) studies in the presence of 1.2 M TFE reveal that **1**−**5** produce CO with excellent faradaic efficiencies (≥90%) and turnover numbers (Figures S42−S46, Table S8); by contrast, complex **6** is a poor catalyst with low faradic efficiency (36%), producing negligible amounts of CO or other common CO_2 reduction products, such as hydrogen or formic acid. The titration results, coupled with results from CPE, indicate that complexes **1**−**5** are competent catalysts, thus allowing for direct comparison of their catalytic performance.

Interestingly, a linear correlation is observed between the catalytic rate constant and the number of secondary amines on the metal complex for **1**−**5** (Figure 2a), suggesting that the pendant secondary amines play a critical role in catalysis. Because the measured rates for **3** and **4** are similar, we hypothesize that the pendant secondary amines act in a noncooperative manner, since the differing orientation of the pendant amines in these complexes has no effect on the catalytic rate. The rates in Figure 2a vary linearly with the number of pendant amines minus one, consistent with a model in which one pendant amine is singly deprotonated and unable to donate a hydrogen bond; complex **5** (which has only one secondary amine) operates at the same rate as complex **6** and 100 times slower than complexes **3** and **4**. We also note that the $Co^{(I)}/Co^{(0)}$ reduction potential in complexes **1**−**5** does not correlate with catalytic performance (Table 1), suggesting that other factors govern the catalytic activity of these cobalt aminopyridine complexes.[40,41]

Taken together, the experimental results begin to paint a picture of the CO_2 reduction mechanism. Linear rate dependence on both [CO_2] and [TFE] indicates that the reaction is first order in each, and the observation of a positive shift in onset potential with the addition of CO_2, but not TFE, indicates favorable binding between the complex and CO_2. The hydrogen kinetic isotope effect (k_H/k_D) of 1.4(2) suggests that protons are involved in the RLS. Finally, the linear rate dependence of the catalytic rate on the number of pendant secondary amines indicates that they play a central role in the reaction mechanism. However, key mechanistic details remain unresolved, including the precise manner in which the pendant proton donors facilitate the catalytic mechanism, the nature of the CO_2 preassociation with the complex, and the competition between inter- and intramolecular proton-transfer steps in the reduction of CO_2; DFT calculations are employed in the following sections to address these points.

Formation of the CO_2-Bound Preassociation Complex. DFT calculations are used to examine the structure and energetics of the CO_2-bound preassociation complex suggested by the electrochemical experiments. Initially focusing on **1**, the geometry of the CO_2-bound complex is optimized in its various accessible oxidation states (corresponding to $\mathbf{1}^{(II)}$, $\mathbf{1}^{(I)}$, and $\mathbf{1}^{(0)}$ for the unbound complex). Of these, only $\mathbf{1}^{(0)}$ has a stable minimum when bound with CO_2, consistent with the Nernstian shifts in Figure S20. In this bound complex, CO_2 binds to the metal center via the carbon atom with a bond length of 2.06 Å, with the pendant amines pointed away from the CO_2 binding site (inset of Figure 2b). Upon binding, charge transfers from the Co center to the CO_2, leading to oxidation of the metal center to a +1 state and a bent CO_2 geometry like that of the gas-phase anion. The anionic character of the bound CO_2 is further supported by CHELPG charge analysis[42] (Table S9).

We now examine the role of the pendant amine protons in CO_2 binding. Previous studies have shown that intramolecular hydrogen bonds can stabilize the bound CO_2.[17,18,43] In principle, such interactions are available in complex $\mathbf{1}^{(I)}$−CO_2 if the pendant secondary amines undergo umbrella flipping to orient their protons toward the bound CO_2. To test this possibility, we compute the energetics and barriers for the conformational change associated with forming either one or two hydrogen bonds between the pendant amine protons and the CO_2 ligand. The structure without intramolecular hydrogen

DOI: 10.1021/acscentsci.7b00607
ACS Cent. Sci. 2018, 4, 397−404

bonds is the most stable, with formation of a single hydrogen bond incurring a cost of 5.2 kcal/mol with a barrier of 10.7 kcal/mol, and with the second hydrogen bond incurring a further 1.3 kcal/mol energy cost with a barrier of 7.2 kcal/mol (Figure S49). Factors contributing to the unfavorability of hydrogen-bond formation include ring strain in the ligand scaffold, the need to rotate CO_2 into a sterically unfavorable configuration, and the relatively weak hydrogen-bond interactions. Although this mode of binding differs from that seen previously in iron porphyrins,[18] it is confirmed by embedded multireference configuration interaction singles and doubles calculations (see Supporting Information).[41,44]

To examine the effect of methyl substitution on the binding of CO_2, we repeat the binding-energy calculations for complexes $\mathbf{2}^{(I)}$–CO_2 through $\mathbf{6}^{(I)}$–CO_2. All six bound complexes are isostructural, with Co–C bond lengths ranging between 2.06 and 2.17 Å (Table S9). The possibility of intramolecular hydrogen bonding was also considered in all five NH-containing complexes and was found to be similarly unfavorable in all cases.

In terms of CO_2 binding, the main difference among complexes **1**–**6** is the degree to which steric repulsions are incurred between CO_2 and the methyl groups, which weakens CO_2 binding. Complex $\mathbf{1}^{(I)}$–CO_2 has a CO_2 binding energy of −11.8 kcal/mol, whereas methylation of all four secondary amines as in complex $\mathbf{6}^{(I)}$–CO_2 results in a binding strength of −0.4 kcal/mol. These weakened binding strengths lead to reduced populations of $\mathbf{X}^{(I)}$–CO_2 preassociation complexes, which manifests as a multiplicative factor in the rate under the assumption that the mechanism proceeds via a CO_2-bound preassociation complex. Specifically, we expect the catalytic rate to be exponential in the CO_2 binding energy, ΔG_X^b

$$k_{\mathrm{obs,X}} \propto \exp\left(-\frac{\Delta G_X^b}{kT}\right)$$

Figure 2b tests the assumption that the catalytic mechanism proceeds via a CO_2-bound preassociation complex by plotting the relationship between the catalytic rate constant and the computed CO_2 binding energy for complexes **1**–**6**. For the complexes that exhibit at least one available pendant proton (i.e., **1**–**4**), the rate is exponential with the CO_2 binding energy, supporting a mechanism that involves formation of CO_2-bound preassociation complex. According to the trend from complexes **1**–**4** in Figure 2b, complexes **5** and **6** also bind CO_2 sufficiently well to perform catalysis. However, as is discussed in the next sections, complexes **5** and **6** are unable to employ the same catalytic pathway as **1**–**4** due to the absence of an available pendant proton. As mentioned previously, the measured pK_a values of complexes $\mathbf{1}^{(II)}$–$\mathbf{5}^{(II)}$ range between 2.48 and 3.10 (Table 1), whereas the pK_a of TFE in DMSO is 23.5.[45] Therefore, complexes $\mathbf{1}^{(II)}$–$\mathbf{5}^{(II)}$ are expected to be singly deprotonated in solution, reducing the number of pendant protons available for catalysis by one. Additionally, computational studies on $\mathbf{1}^{(II)}$ estimate that its second deprotonation would correspond to a pK_a of 5.2, and its third deprotonation would correspond to a pK_a of 14.0. However, these additional pK_a values cannot be measured experimentally, due to the decomposition observed at pH above 3.5.

Nature of the Rate-Limiting Protonation Step. Following binding, CO_2 must be twice protonated to complete the catalytic cycle. Previous work on an analogous cobalt tetraazamacrocyclic complex indicates that this process proceeds sequentially, with the first protonation forming a COOH ligand and the second protonation cleaving the C–OH bond to form water and bound CO.[46] In this work, the previously discussed experimental results suggest that a proton-involving step is rate-limiting for the overall catalytic cycle. We now use computation to investigate the various available protonation pathways.

Reaction energies of $\mathbf{X}^{(I)}$–CO_2 (**X** = **1**–**6**) with a proton from solution to yield $\mathbf{X}^{(II)}$–CO_2H are computed with reference to the experimental free energy of solvation of the proton in DMSO (details in Supporting Information). The overall energy of this reaction ranges from −9.0 kcal/mol (complex $\mathbf{1}^{(I)}$–CO_2) to −18.2 kcal/mol (complex $\mathbf{3}^{(I)}$–CO_2).

Having completed two reduction steps and a first protonation step, the catalytic cycle could involve either further protonation ("EECC" mechanism, Figure 3, where E = electrochemical, and C = chemical step) or reduction of $\mathbf{1}^{(II)}$–CO_2H followed by protonation ("(E)ECEC" mechanism, Figure S53). Because the reduction of $Co^{(I)}$ to $Co^{(0)}$ is irreversible, these mechanisms cannot be experimentally distinguished and calculations are instead employed. The 1-electron reduction potential of $\mathbf{1}^{(II)}$–CO_2H is calculated to be −2.9 V vs $Fc^{+/0}$, suggesting that reduction of $\mathbf{1}^{(II)}$–CO_2H is not kinetically competent at the potential of maximum catalytic current (−2.7 V vs $Fc^{+/0}$). This, along with precedent from the aforementioned results of ,[46] suggests that the EECC mechanism is dominant; the alternative (E)ECEC mechanism is further detailed in the Supporting Information.

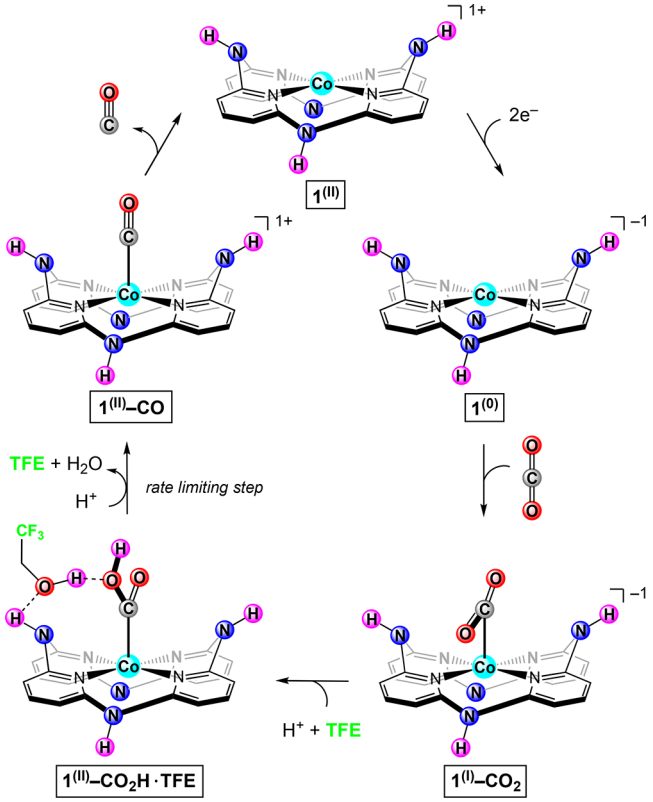

Figure 3. Proposed EECC catalytic cycle illustrated with complex **1**, where E = electrochemical, and C = chemical step.

Proceeding along the EECC mechanism, the second protonation may occur either on the protonated oxygen to form a $CO(OH_2)$ adduct or on the unprotonated oxygen to

DOI: 10.1021/acscentsci.7b00607
ACS Cent. Sci. 2018, 4, 397–404

form a $C(OH)_2$ adduct. Calculations for $\mathbf{1}^{(II)}$–$CO(OH_2)$ and $\mathbf{1}^{(II)}$–$C(OH)_2$ show that the latter is less favorable by 26.4 kcal/mol, eliminating it from the catalytic pathway. After the second protonation, the C–OH bond in $\mathbf{X}^{(II)}$–$CO(OH_2)$ spontaneously breaks, forming $\mathbf{X}^{(II)}$–CO and water. The energy of this reaction ranges from −8.4 kcal/mol (complex $\mathbf{1}^{(II)}$–CO_2H) to −10.4 kcal/mol (complex $\mathbf{6}^{(II)}$–CO_2H).

Figure 4 shows a comparison of the overall thermodynamic driving force between the first and second protonations for complexes **1**–**6**. The clustering of complexes **1** and **2** versus **3**–**6** is believed to be due to solvation. This is further discussed in the Supporting Information section titled "Effect of solubility on the first protonation energy." In all six complexes, the second protonation is less favorable, consistent with previous studies on iron porphyrin complexes.[18] This result can be understood as a difference in nucleophilicity between the CO_2 and COOH intermediates, with the CO_2 ligand exhibiting greater anionic character (Tables S9 and S11). Though activation barriers were not calculated, the Bell–Evans–Polanyi principle suggests that the energetically less favorable second protonation will likewise have a slower reaction rate. In summary, we argue that $\mathbf{X}^{(I)}$–CO_2 is twice protonated on the same oxygen via the EECC mechanism to form water and $\mathbf{X}^{(II)}$–CO, with the second of these protonation steps constituting the RLS.

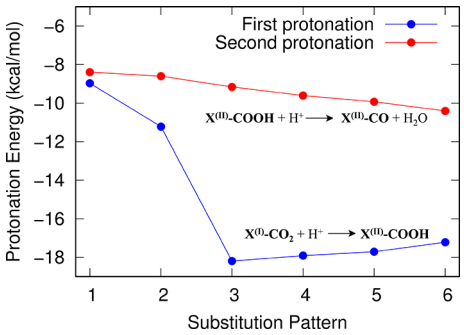

Figure 4. Protonation energies of complexes $\mathbf{1}^{(I)}$–CO_2 through $\mathbf{6}^{(I)}$–CO_2 (blue) and $\mathbf{1}^{(II)}$–CO_2H through $\mathbf{6}^{(II)}$–CO_2H (red).

Intra- versus Intermolecular Proton Transfer for the Rate-Limiting Step. Having identified the second protonation of the CO_2 ligand as the likely RLS, we now investigate whether protonation is more favorable via an intra- vs intermolecular mechanism. Our experimental observations constrain this mechanism in three ways, with (i) titrations indicating that the RLS involves undissociated TFE, (ii) the overall catalytic rates for complexes **1**–**6** suggesting that the RLS involves the pendant secondary amines in a noncooperative manner, and (iii) the H/D KIE indicating that the RLS involves protons.

Two mechanisms consistent with these observations include intramolecular acid-assisted proton transfer from the pendant amine to COOH and intermolecular pendant amine assisted proton transfer from the acid to the COOH. For the intramolecular mechanism, proton transfer follows rotation of the COOH ligand and umbrella-flipping of the pendant amine to form a hydrogen-bonding geometry (Figure 5); this conformational rearrangement is energetically uphill by 10.3 kcal/mol with a barrier of 15.2 kcal/mol, and the subsequent proton transfer step has a barrier of 3.9 kcal/mol. The high energy barrier for reaching the intermediate disfavors this mechanism, as does the fact that inclusion of a bound acid molecule in the calculations further destabilizes the intermediate by 1.1 kcal/mol, contradicting the experimental trend of increasing rate with increasing acid concentration (Figures S51 and S52).

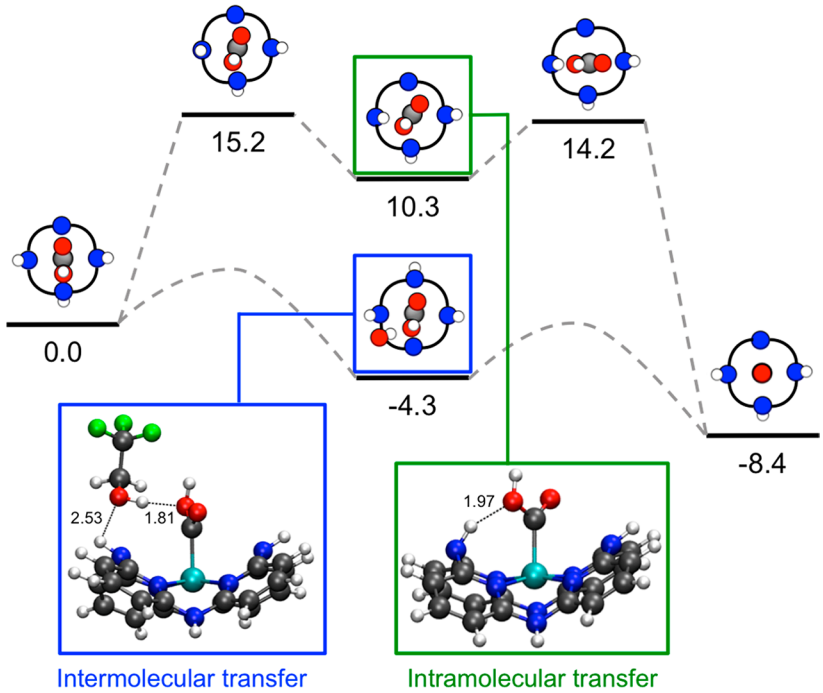

Figure 5. Two pathways for the rate-limiting protonation of complex $\mathbf{1}^{(II)}$–CO_2H. Geometries of critical points are shown and labeled by their energies in kcal/mol. Below: side view of a key intermediate from each pathway. Hydrogen bonds are labeled with dashed lines, and their lengths are given in ångstroms. Fluorine atoms are shown in green.

DOI: 10.1021/acscentsci.7b00607
ACS Cent. Sci. 2018, 4, 397–404

To investigate the intermolecular proton-transfer mechanism, we consider the structure and energetics of $\mathbf{1}^{(II)}$–CO_2H complex, which contains a TFE molecule bridging the pendant amine and COOH (Figure 5, blue box). Geometry optimization reveals a stable binding energy of 4.3 kcal/mol, and a short (1.81 Å) hydrogen bond, which suggests the favorability of intermolecular proton transfer to the COOH ligand. Note that the amine–acid hydrogen-bond distance is too long to support a shuttle mechanism in which a proton is transferred from the amine to the acid simultaneous with proton transfer from the acid to the COOH ligand. We thus conclude that the second protonation proceeds via direct proton transfer from TFE to the COOH ligand, assisted by the pendant amine proton. Table S12 confirms that this analysis is consistent with the previous section, indicating that all of the corresponding barriers and intermediates shown in Figure 5 are lower in energy when considering the first protonation step.

DISCUSSION

Figure 3 summarizes the proposed catalytic mechanism that emerges from the combined analysis. Complex $\mathbf{X}^{(II)}$ ($\mathbf{X} = \mathbf{1}$–$\mathbf{6}$) is reduced by two electrons and binds CO_2 to yield $\mathbf{X}^{(I)}$–CO_2. The CO_2 adduct is twice protonated, with the latter being rate-limiting and occurring via an intermolecular mechanism that is noncooperatively facilitated by the pendant amines. Finally, the C–OH_2 bond spontaneously cleaves to release water, and CO dissociates from $\mathbf{X}^{(II)}$–CO to regenerate the catalyst.

Given this mechanism, the overall catalytic rate for complex $\mathbf{X}$ ($k_{obs,X}$) is

$$k_{obs,\mathbf{X}} = ((n_{\mathbf{X}} - 1)[\mathrm{TFE}]k_{RLS}) \times ([\mathbf{X}][CO_2]\, e^{-\Delta G_{\mathbf{X}}^{b}/kT})$$

where k_{RLS} is the rate constant of the RLS per pendant amine proton irrespective of $\mathbf{X}$, $(n_{\mathbf{X}} - 1)$ is the number of available amine protons in $\mathbf{X}$, $[\mathbf{X}]$ is the concentration of $\mathbf{X}$, and $\Delta G_{\mathbf{X}}^{b}$ is the free energy of CO_2 binding. The first grouping of terms summarizes the kinetics of the rate-limiting step, and the second summarizes the binding of CO_2 to form the preassociation complex. A derivation of this rate equation can be found in the Supporting Information section titled "Kinetics of the EECC mechanism."

For the rate-limiting step, each pendant amine can noncooperatively bind an acid molecule, activating and enhancing the local concentration of proton donors around the COOH adduct. The noncooperative nature of this hydrogen bonding makes the degree of catalytic enhancement dependent only on the number of available pendant proton donors, such that k_{RLS} is independent of the number of pendant amines (Figure 2a).

The second grouping of terms in the rate expression represents the thermodynamics of CO_2 binding to form the preassociation complex. As seen in Figure 2b, the experimental catalytic rate is exponentially related to the computed CO_2 binding free energy for complexes **1**–**4**. This trend does not extend to complexes **5** and **6** where the first grouping of terms sets the overall rate to zero, due to the absence of an available pendant proton.

CONCLUSIONS

We introduce and characterize a series of cobalt aminopyridine complexes that vary as a function of the number of pendant proton donors and allow for the well-controlled analysis of contributions from the first and second coordination spheres in CO_2 reduction catalysis. Electrochemical studies show that the CO_2 reduction activity of these complexes depends strongly on the number of secondary amines incorporated in the ligand framework. The observed linear dependence of the rate of catalysis on the number of pendant proton donors has not been previously reported for CO_2 reduction. Computational studies reveal the mechanism by which the pendant amines facilitate rate-limiting intermolecular proton transfer via noncooperative hydrogen bonds to acid in solution. By enabling systematic control over the number of proton relays present in the second coordination sphere, the reported complexes provide a relevant model for biological systems and homogeneous catalysts for small molecule activation. Furthermore, these complexes offer a framework for tuning the effect of the second coordination sphere on CO_2 reduction, and more generally, on multi-electron, multiproton reduction reactions.

ASSOCIATED CONTENT

Supporting Information

The Supporting Information is available free of charge on the ACS Publications website at DOI: 10.1021/acscentsci.7b00607.

Experimental details and crystallographic data (PDF)
Crystallographic data for $\mathbf{2}^{(II)}$ (CIF)
Crystallographic data for $\mathbf{3}^{(II)}$ (CIF)
Crystallographic data for $\mathbf{4}^{(II)}$ (CIF)
Crystallographic data for $\mathbf{5}^{(II)}$ (CIF)

CCDC 1590218–1590221 contain the supplementary crystallographic data for this manuscript. These data can be obtained free of charge via www.ccdc.cam.ac.uk/data_request/cif, or by emailing data_request@ccdc.cam.ac.uk, or by contacting The Cambridge Crystallographic Data Centre, 12 Union Road, Cambridge CB2 1EZ, UK; fax: + 44 1223 336033.

AUTHOR INFORMATION

Corresponding Authors

*E-mail: smarines@usc.edu.
*E-mail: tfm@caltech.edu.

ORCID

Thomas F. Miller III: 0000-0002-1882-5380
Smaranda C. Marinescu: 0000-0003-2106-8971

Author Contributions

‡A.C. and M.W.: equal contribution.

Notes

The authors declare no competing financial interest.

ACKNOWLEDGMENTS

This work was supported by the University of Southern California and the National Science Foundation (NSF) through the CAREER award (CHE-1555387) and the Chemistry of Life Processes Program (CHE-1611581). This material is based upon work performed by the Joint Center for Artificial Photosynthesis, a DOE Energy Innovation Hub, supported through the Office of Science of the U.S. Department of Energy under Award Number DE-SC0004993. We are grateful to the USC Wrigley Institute for a Norma and Jerol Sonosky summer fellowship to A.C. M.W. thanks the Resnick Sustainability Institute for a postdoctoral fellowship. We are grateful to NSF (Grant CRIF 1048807) and USC for their sponsorship of NMR spectrometers and an X-ray diffractometer.

DOI: 10.1021/acscentsci.7b00607
ACS Cent. Sci. 2018, 4, 397–404

REFERENCES

(1) Benson, E. E.; Kubiak, C. P.; Sathrum, A. J.; Smieja, J. M. Electrocatalytic and homogeneous approaches to conversion of CO_2 to liquid fuels. *Chem. Soc. Rev.* **2009**, *38*, 89−99.

(2) Appel, A. M.; Bercaw, J. E.; Bocarsly, A. B.; Dobbek, H.; DuBois, D. L.; Dupuis, M.; Ferry, J. G.; Fujita, E.; Hille, R.; Kenis, P. J. A.; Kerfeld, C. A.; Morris, R. H.; Peden, C. H. F.; Portis, A. R.; Ragsdale, S. W.; Rauchfuss, T. B.; Reek, J. N. H.; Seefeldt, L. C.; Thauer, R. K.; Waldrop, G. L. Frontiers, Opportunities, and Challenges in Biochemical and Chemical Catalysis of CO_2 Fixation. *Chem. Rev.* **2013**, *113*, 6621−6658.

(3) Morris, A. J.; Meyer, G. J.; Fujita, E. Molecular Approaches to the Photocatalytic Reduction of Carbon Dioxide for Solar Fuels. *Acc. Chem. Res.* **2009**, *42*, 1983−1994.

(4) Rakowski Dubois, M.; Dubois, D. L. Development of Molecular Electrocatalysts for CO_2 Reduction and H_2 Production/Oxidation. *Acc. Chem. Res.* **2009**, *42*, 1974−1982.

(5) Collin, J. P.; Sauvage, J. P. Electrochemical reduction of carbon dioxide mediated by molecular catalysts. *Coord. Chem. Rev.* **1989**, *93*, 245−268.

(6) Costentin, C.; Robert, M.; Savéant, J. M. Catalysis of the electrochemical reduction of carbon dioxide. *Chem. Soc. Rev.* **2013**, *42*, 2423−2436.

(7) Savéant, J. M. Molecular Catalysis of Electrochemical Reactions. Mechanistic Aspects. *Chem. Rev.* **2008**, *108*, 2348−2378.

(8) Takeda, H.; Cometto, C.; Ishitani, O.; Robert, M. Electrons, Photons, Protons and Earth-Abundant Metal Complexes for Molecular Catalysis of CO_2 Reduction. *ACS Catal.* **2017**, *7*, 70−88.

(9) Schneider, J.; Jia, H.; Muckerman, J. T.; Fujita, E. Thermodynamics and kinetics of CO_2, CO, and H^+ binding to the metal centre of CO_2 reduction catalysts. *Chem. Soc. Rev.* **2012**, *41*, 2036−2051.

(10) Ragsdale, S. W.; Kumar, M. Nickel-Containing Carbon Monoxide Dehydrogenase/Acetyl-CoA Synthase. *Chem. Rev.* **1996**, *96*, 2515−2540.

(11) Jeoung, J.-H.; Dobbek, H. Carbon Dioxide Activation at the Ni,Fe-Cluster of Anaerobic Carbon Monoxide Dehydrogenase. *Science* **2007**, *318*, 1461−1464.

(12) Lubitz, W.; Ogata, H.; Rüdiger, O.; Reijerse, E. Hydrogenases. *Chem. Rev.* **2014**, *114*, 4081−4148.

(13) Berggren, G.; Adamska, A.; Lambertz, C.; Simmons, T. R.; Esselborn, J.; Atta, M.; Gambarelli, S.; Mouesca, J. M.; Reijerse, E.; Lubitz, W.; Happe, T.; Artero, V.; Fontecave, M. Biomimetic assembly and activation of [FeFe]-hydrogenases. *Nature* **2013**, *499*, 66−69.

(14) DuBois, D. L. Development of Molecular Electrocatalysts for Energy Storage. *Inorg. Chem.* **2014**, *53*, 3935−3960.

(15) Rakowski DuBois, M.; DuBois, D. L. The roles of the first and second coordination spheres in the design of molecular catalysts for H_2 production and oxidation. *Chem. Soc. Rev.* **2009**, *38*, 62−72.

(16) Agarwal, J.; Shaw, T. W.; Schaefer, H. F., III; Bocarsly, A. B. Design of a Catalytic Active Site for Electrochemical CO_2 Reduction with Mn(I)-Tricarbonyl Species. *Inorg. Chem.* **2015**, *54*, 5285−5294.

(17) Costentin, C.; Drouet, S.; Robert, M.; Savéant, J. M. A Local Proton Source Enhances CO_2 Electroreduction to CO by a Molecular Fe Catalyst. *Science* **2012**, *338*, 90−94.

(18) Costentin, C.; Passard, G.; Robert, M.; Savéant, J.-M. Pendant Acid−Base Groups in Molecular Catalysts: H-Bond Promoters or Proton Relays? Mechanisms of the Conversion of CO_2 to CO by Electrogenerated Iron(0)Porphyrins Bearing Prepositioned Phenol Functionalities. *J. Am. Chem. Soc.* **2014**, *136*, 11821−11829.

(19) Costentin, C.; Passard, G.; Robert, M.; Savéant, J.-M. Ultraefficient homogeneous catalyst for the CO_2-to-CO electrochemical conversion. *Proc. Natl. Acad. Sci. U. S. A.* **2014**, *111*, 14990−14994.

(20) Costentin, C.; Robert, M.; Savéant, J.-M. Current Issues in Molecular Catalysis Illustrated by Iron Porphyrins as Catalysts of the CO_2-to-CO Electrochemical Conversion. *Acc. Chem. Res.* **2015**, *48*, 2996−3006.

(21) Costentin, C.; Robert, M.; Savéant, J.-M.; Tatin, A. Efficient and selective molecular catalyst for the CO_2-to-CO electrochemical conversion in water. *Proc. Natl. Acad. Sci. U. S. A.* **2015**, *112*, 6882−6886.

(22) Azcarate, I.; Costentin, C.; Robert, M.; Savéant, J.-M. Through-Space Charge Interaction Substituent Effects in Molecular Catalysis Leading to the Design of the Most Efficient Catalyst of CO_2-to-CO Electrochemical Conversion. *J. Am. Chem. Soc.* **2016**, *138*, 16639−16644.

(23) Azcarate, I.; Costentin, C.; Robert, M.; Savéant, J.-M. Dissection of Electronic Substituent Effects in Multielectron−Multistep Molecular Catalysis. Electrochemical CO_2-to-CO Conversion Catalyzed by Iron Porphyrins. *J. Phys. Chem. C* **2016**, *120*, 28951−28960.

(24) Ngo, K. T.; McKinnon, M.; Mahanti, B.; Narayanan, R.; Grills, D. C.; Ertem, M. Z.; Rochford, J. Turning on the Protonation-First Pathway for Electrocatalytic CO_2 Reduction by Manganese Bipyridyl Tricarbonyl Complexes. *J. Am. Chem. Soc.* **2017**, *139*, 2604−2618.

(25) Galan, B. R.; Schöffel, J.; Linehan, J. C.; Seu, C.; Appel, A. M.; Roberts, J. A. S.; Helm, M. L.; Kilgore, U. J.; Yang, J. Y.; Dubois, D. L.; Kubiak, C. P. Electrocatalytic Oxidation of Formate by $[Ni(P^R_2N^{R'}_2)_2(CH_3CN)]^{2+}$ Complexes. *J. Am. Chem. Soc.* **2011**, *133*, 12767−12779.

(26) Seu, C. S.; Appel, A. M.; Doud, M. D.; DuBois, D. L.; Kubiak, C. P. Formate oxidation via β-deprotonation in $[Ni(P^R_2N^{R'}_2)_2(CH_3CN)]^{2+}$ complexes. *Energy Environ. Sci.* **2012**, *5*, 6480−6490.

(27) Roy, S.; Sharma, B.; Pécaut, J.; Simon, P.; Fontecave, M.; Tran, P. D.; Derat, E.; Artero, V. Molecular Cobalt Complexes with Pendant Amines for Selective Electrocatalytic Reduction of Carbon Dioxide to Formic Acid. *J. Am. Chem. Soc.* **2017**, *139*, 3685−3696.

(28) Beley, M.; Collin, J.-P.; Ruppert, R.; Sauvage, J.-P. Nickel(II)-cyclam: an extremely selective electrocatalyst for reduction of CO_2 in water. *J. Chem. Soc., Chem. Commun.* **1984**, 1315−1316.

(29) Beley, M.; Collin, J. P.; Ruppert, R.; Sauvage, J. P. Electrocatalytic reduction of carbon dioxide by nickel $cyclam^{2+}$ in water: study of the factors affecting the efficiency and the selectivity of the process. *J. Am. Chem. Soc.* **1986**, *108*, 7461−7467.

(30) Froehlich, J. D.; Kubiak, C. P. Homogeneous CO_2 Reduction by Ni(cyclam) at a Glassy Carbon Electrode. *Inorg. Chem.* **2012**, *51*, 3932−3934.

(31) Schneider, J.; Jia, H.; Kobiro, K.; Cabelli, D. E.; Muckerman, J. T.; Fujita, E. Nickel(II) macrocycles: highly efficient electrocatalysts for the selective reduction of CO_2 to CO. *Energy Environ. Sci.* **2012**, *5*, 9502−9510.

(32) Fisher, B. J.; Eisenberg, R. Electrocatalytic reduction of carbon dioxide by using macrocycles of nickel and cobalt. *J. Am. Chem. Soc.* **1980**, *102*, 7361−7363.

(33) Fujita, E.; Creutz, C.; Sutin, N.; Brunschwig, B. S. Carbon Dioxide Activation by Cobalt Macrocycles: Evidence of Hydrogen Bonding between Bound CO_2 and the Macrocycle in Solution. *Inorg. Chem.* **1993**, *32*, 2657−2662.

(34) Zilbermann, I.; Winnik, M.; Sagiv, D.; Rotman, A.; Cohen, H.; Meyerstein, D. Properties of monovalent nickel complexes with tetraaza-macrocyclic ligands in aqueous solutions. *Inorg. Chim. Acta* **1995**, *240*, 503−514.

(35) Bujno, K.; Bilewicz, R.; Siegfried, L.; Kaden, T. A. Effects of ligand structure on the adsorption of nickel tetraazamacrocyclic complexes and electrocatalytic CO_2 reduction. *J. Electroanal. Chem.* **1998**, *445*, 47−53.

(36) Chapovetsky, A.; Do, T. H.; Haiges, R.; Takase, M. K.; Marinescu, S. C. Proton-Assisted Reduction of CO_2 by Cobalt Aminopyridine Macrocycles. *J. Am. Chem. Soc.* **2016**, *138*, 5765−5768.

(37) Zhang, E.-X.; Wang, D.-X.; Huang, Z.-T.; Wang, M.-X. Synthesis of $(NH)_m(NMe)_{4-m}$-Bridged Calix[4]pyridines and the Effect of NH Bridge on Structure and Properties. *J. Org. Chem.* **2009**, *74*, 8595−8603.

(38) Drew, M. G. B.; Nag, S.; Datta, D. Acid dissociation of 2,2′-dipyridylamine in non-aqueous medium when chelated to some $Ru(II)N_4$ cores. *Inorg. Chim. Acta* **2008**, *361*, 417−421.

DOI: 10.1021/acscentsci.7b00607
ACS Cent. Sci. 2018, 4, 397−404

(39) Fujita, E.; Creutz, C.; Sutin, N.; Szalda, D. J. Carbon dioxide activation by cobalt(I) macrocycles: factors affecting carbon dioxide and carbon monoxide binding. *J. Am. Chem. Soc.* **1991**, *113*, 343−353.
(40) Pegis, M. L.; Wise, C. F.; Koronkiewicz, B.; Mayer, J. M. Identifying and Breaking Scaling Relations in Molecular Catalysis of Electrochemical Reactions. *J. Am. Chem. Soc.* **2017**, *139*, 11000−11003.
(41) Huo, P.; Uyeda, C.; Goodpaster, J. D.; Peters, J. C.; Miller, T. F. Breaking the Correlation between Energy Costs and Kinetic Barriers in Hydrogen Evolution via a Cobalt Pyridine-Diimine-Dioxime Catalyst. *ACS Catal.* **2016**, *6*, 6114−6123.
(42) Breneman, C. M.; Wiberg, K. B. Determining atom-centered monopoles from molecular electrostatic potentials. The need for high sampling density in formamide conformational analysis. *J. Comput. Chem.* **1990**, *11*, 361−373.
(43) Fujita, E.; Szalda, D. J.; Creutz, C.; Sutin, N. Carbon dioxide activation: thermodynamics of carbon dioxide binding and the involvement of two cobalt centers in the reduction of carbon dioxide by a cobalt(I) macrocycle. *J. Am. Chem. Soc.* **1988**, *110*, 4870−4871.
(44) Manby, F. R.; Stella, M.; Goodpaster, J. D.; Miller, T. F., III A Simple, Exact Density-Functional-Theory Embedding Scheme. *J. Chem. Theory Comput.* **2012**, *8*, 2564−2568.
(45) Bordwell, G. F. Equilibrium Acidities in Dimethyl Sulfoxide Solution. *Acc. Chem. Res.* **1988**, *21*, 456−463.
(46) Fujita, E.; Furenlid, L. R.; Renner, M. W. Direct XANES evidence for charge transfer in Co-CO_2 complexes. *J. Am. Chem. Soc.* **1997**, *119*, 4549−4550.

DOI: 10.1021/acscentsci.7b00607
ACS Cent. Sci. 2018, 4, 397−404